Radiology

ORIGINAL RESEARCH • NEURORADIOLOGY

MRI Atlas of IDH Wild-Type Supratentorial Glioblastoma: Probabilistic Maps of Phenotype, Management, and Outcomes

Alexandre Roux, MD, MSc • Pauline Roca, PhD • Myriam Edjlali, MD, PhD • Kanako Sato, MD • Marc Zanello, MD, MSc • Edouard Dezamis, MD, MSc • Pietro Gori, PhD • Stéphanie Lion, MSc • Ariane Fleury, MSc • Frédéric Dhermain, MD, PhD • Jean-François Meder, MD, PhD • Fabrice Chrétien, MD, PhD • Emmanuèle Lechapt, MD, PhD • Pascale Varlet, MD, PhD • Catherine Oppenheim, MD, PhD • Johan Pallud, MD, PhD

From the Department of Neurosurgery, Sainte-Anne Hospital, Paris, France (A.R., M.Z., E.D., J.P.); Paris Descartes University, Sorbonne Paris Cité, Paris, France (A.R., P.R., M.E., M.Z., J.F.M., F.C., E.L., P.V., C.O., J.P.); UMR 1266 INSERM, IMA-BRAIN, Institute of Psychiatry and Neurosciences of Paris, Paris, France (A.R., P.R., M.E., K.S., M.Z., P.G., S.L., A.F., J.F.M., P.V., C.O., J.P.); Department of Neuroradiology, Sainte-Anne Hospital, Paris, France (M.E., J.F.M., C.O.); Department of Radiology, Juntendo University School of Medicine, Tokyo, Japan (K.S.); LTCI, Telecom ParisTech, Paris, France (P.G.); Department of Radiotherapy, Gustave Roussy University Hospital, Villejuif, France (F.D.); and Department of Neuropathology, Sainte-Anne Hospital, Paris, France (F.C., E.L., P.V.). Received March 6, 2019; revision requested May 17; revision received August 17; accepted August 27. **Address correspondence to** J.P. (e-mail: *johanpallud@hotmail.com*).

Conflicts of interest are listed at the end of this article.

See also the editorial by Huang in this issue.

Radiology 2019; 00:1–11 • https://doi.org/10.1148/radiol.2019190491 • Content codes: MR NR

Background: Tumor location is a main prognostic parameter in patients with glioblastoma. Probabilistic MRI-based brain atlases specifying the probability of tumor location associated with important demographic, clinical, histomolecular, and management data are lacking for isocitrate dehydrogenase (IDH) wild-type glioblastomas.

Purpose: To correlate glioblastoma location with clinical phenotype, surgical management, and outcomes by using a probabilistic analysis in a three-dimensional (3D) MRI-based atlas.

Materials and Methods: This retrospective study included all adults surgically treated for newly diagnosed IDH wild-type supratentorial glioblastoma in a tertiary adult surgical neuro-oncology center (2006–2016). Semiautomated tumor segmentation and spatial normalization procedures to build a 3D MRI-based atlas were validated. The authors performed probabilistic analyses by using voxel-based lesion symptom mapping technology. The Liebermeister test was used for binary data, and the generalized linear model was used for continuous data.

Results: A total of 392 patients (mean age, 61 years ± 13; 233 men) were evaluated. The authors identified the preferential location of glioblastomas according to subventricular zone, age, sex, clinical presentation, revised Radiation Therapy Oncology Group-Recursive Partitioning Analysis class, Karnofsky performance status, O^6-methylguanine DNA methyltransferase promoter methylation status, surgical management, and survival. The superficial location distant from the eloquent area was more likely associated with a preserved functional status at diagnosis (348 of 392 patients [89%], $P < .05$), a large surgical resection (173 of 392 patients [44%], $P < .05$), and prolonged overall survival (163 of 334 patients [49%], $P < .05$). In contrast, deep location and location within eloquent brain areas were more likely associated with an impaired functional status at diagnosis (44 of 392 patients [11%], $P < .05$), a neurologic deficit (282 of 392 patients [72%], $P < .05$), treatment with biopsy only (183 of 392 patients [47%], $P < .05$), and shortened overall survival (171 of 334 patients [51%], $P < .05$).

Conclusion: The authors identified the preferential location of isocitrate dehydrogenase wild-type glioblastomas according to parameters of interest and provided an image-based integration of multimodal information impacting survival results. This suggests the role of glioblastoma location as a surrogate and multimodal parameter integrating several known prognostic factors.

Online supplemental material is available for this article.

Isocitrate dehydrogenase (IDH) wild-type glioblastoma (World Health Organization grade IV astrocytoma) is the most common malignant primary brain tumor in adults (1). Tumor location is a key parameter in the care of patients with glioblastoma because it correlates with demographic characteristics, clinical presentation, histomolecular characteristics, surgical management, delivery of subsequent oncologic treatments, and, therefore, outcomes (2–6). Improvements in imaging after treatment improves the accuracy of neuro-anatomic studies owing to a voxel-based analysis and enables correlation studies. Such probabilistic MRI-based brain atlases have been developed for diffuse low-grade gliomas, including a proposal of a resection probability map (7,8), and high-grade gliomas, including histomolecular findings (9–12), but is lacking for IDH wild-type glioblastomas.

Focusing on patients with supratentorial newly diagnosed IDH wild-type glioblastomas in adults in current practice and who received modern standard-of-care treatment (13), we aimed to assess the correlation between tumor location and *(a)* clinical presentation (age, symptoms, Karnofsky performance status), *(b)* surgical management

Abbreviations

CI = confidence interval, IDH = isocitrate dehydrogenase, MGMT = O^6-methylguanine DNA methyltransferase, OS = overall survival, PFS = progression-free survival, RTOG-RPA = revised Radiation Therapy Oncology Group–Recursive Partitioning Analysis, 3D = three-dimensional

Summary

An MRI glioblastoma atlas provides integration of multimodal parameters impacting survival results and indicates preferential location according to parameters of interest, including subventricular zone, age, sex, and clinical presentation.

Key Results

- We developed a three-dimensional atlas of glioblastoma location from a clinical, imaging, and histopathologic database of 392 adults with newly diagnosed isocitrate dehydrogenase wild-type supratentorial glioblastomas.
- Superficial tumor location (distant from the eloquent area) was associated with preserved functional status at diagnosis (11% of patients, $P < .05$), large surgical resection (44% of patients, $P < .05$), and prolonged survival (49% of patients, $P < .05$).
- Deep tumor location and the location within eloquent brain areas were associated with impaired functional status at diagnosis (11% of patients, $P < .05$), neurologic deficit (72% of patients, $P < .05$), surgical treatment limited to biopsy (47% of patients, $P < .05$), and shortened survival (51% of patients, $P < .05$).

(feasibility of a surgical resection, extent of resection), *(c)* imaging and histomolecular findings (involvement of the subventricular zone, O^6-methylguanine DNA methyltransferase [MGMT] promoter methylation status), and *(d)* outcomes (progression-free survival [PFS] and overall survival [OS]).

Materials and Methods

The authors had full control of the data and information presented for publication. The authors report no conflicts of interest. We have not included any patients previously analyzed in another study on this topic.

This study was authorized by the French National Data Information and Freedom Commission (CNIL, reference number: DE-2017–079) and the local ethics committee (CPP Ile-de-France 6, reference number: n°2017-A02324–49, CPP/63–17). The requirement to obtain informed consent was waived for this observational retrospective study in accordance with French legislation.

Data Source

We identified consecutive patients treated for a glioblastoma in a tertiary adult surgical neuro-oncology center. Inclusion criteria were as follows: *(a)* patients at least 18 years of age; *(b)* newly diagnosed glioblastoma; *(c)* supratentorial location; *(d)* MRI performed in our institution; *(e)* diagnosis of IDH wild-type glioblastoma on the basis of blinded neuropathologic reassessment performed previously by one evaluator (E.L.Z., with 15 years of experience) according to the 2016 World Health Organization classification (including the search for diffuse midline H3 K27M-mutant high-grade glioma by using immunohistochemistry, and the *IDH1*/2 sequencing following negative R132H IDH1 immunohistochemistry in glioblastomas from patients younger than 55 years) (1); and *(f)* postoperative modern standard-of-care treatment (13). Between January 2006 and December 2016, 533 patients were screened; 392 patients were included in our study (see patient flowchart in Fig 1).

Imaging Processing

MRI protocol.—We performed contrast material–enhanced three-dimensional (3D) T1-weighted fast spoiled gradient-recalled acquisition (gadoterate meglumine [Dotarem; Guerbet, Aulnay-sous-Bois, France], 0.1 mmol/kg) with either a 1.5-T (Signa EchoSpeed; GE Healthcare, Milwaukee, Wis) or 3-T (MR 750, GE Healthcare) MRI scanner. The imaging parameters for 1.5-T imaging were as follows: repetition time msec/echo time msec, 10.2/3.4; field of view, 24 cm; section thickness, 1.2 mm; and section spacing, 0.5 mm. The imaging parameters for 3-T MRI were as follows: 10.2/3.4; field of view, 22 cm; section thickness, 1.2 mm; and section spacing, 0.0 mm.

MRI database organization.—We anonymized all MRI files and converted them to Neuroimaging Informatics Technology Initiative format. We organized the imaging database according to the Brain Imaging Data Structure international standard for organizing and describing MRI data sets (*http://bids.neuroimaging.io*).

Glioblastoma segmentation.—One evaluator (A.R., with 4 years of experience), who was blinded to clinical, histomolecular, and follow-up data, segmented glioblastoma components on preoperative images with use of open-source Multi-Image Analysis GUI software (2016, MANGO software, version 4.0.1; Research Imaging Institute, University of Texas Health Science Center, San Antonio, *http://ric.uthscsa.edu/mango/*) and designed several semiautomated scripts from the macro command. We summed enhancing and necrotic components to form the whole solid tumor component, which constituted the subsequent region of interest (Fig E1 [online]). We established the extent of resection by quantifying the volume of residual tumor on postoperative (within 48 hours) 3D T1-weighted fast spoiled gradient-recalled images.

MRI coregistration and normalization.—We performed MRI registration by using open-source software (Statistical Parametric Mapping 12, 2014; Functional Imaging Laboratory, Wellcome Trust Centre for Neuroimaging–Institute of Neurology, University College London, England) running on MATLAB (R2018a; MathWorks, Natick, Mass). We registered MRI scans to a 1.0-mm isotropic brain atlas (Montreal Neurologic Institute, or MNI, 152 space) with the open-source Clinical Toolbox tool (2017, Department of Psychology, University of South Carolina, Columbia, SC) and the Diffeomorphic Anatomic Registration Using Exponentiated Lie Algebra open-source tool (2018, Wellcome Trust Centre for Neuroimaging) (14). We introduced a cost-function masking approach (15), which provides better and more reliable matching to the Montreal Neurologic Institute template for lesioned brains (14). To

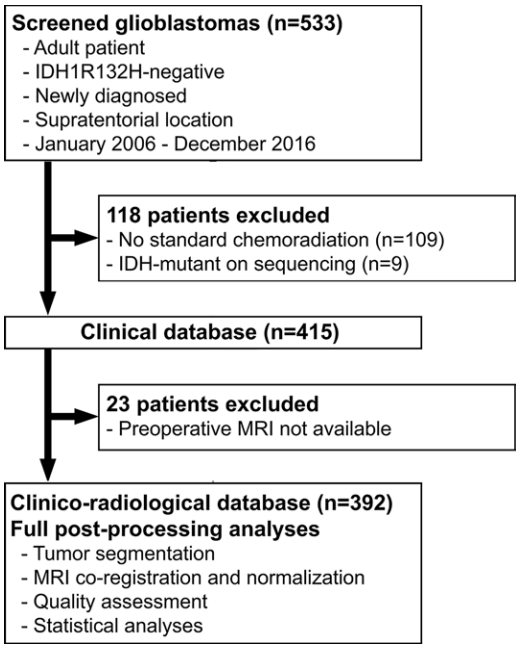

Figure 1: Flowchart shows details of patient selection process. IDH = isocitrate dehydrogenase.

define the cost-function mask, we used a binary mask of the segmented glioblastoma.

***Quality assessment.*—**We assessed the quality of the segmentation and of the spatial normalization by means of visual inspection. To check the standardization procedure, we introduced a quality control method (8,16). An external evaluator (K.S., with 8 years of experience), blinded to clinical, histomolecular, and follow-up data, performed another segmentation by using a random selection of 49 of the 392 patients (12%). We checked the quality of the spatial normalization by selecting nine parenchymal points (Fig E2 [online]) on both the Montreal Neurologic Institute template and target brains. We performed the clinical validation by comparing previously published maps of glioblastoma location by sex and Karnofsky performance status at diagnosis (11,17) with the maps we obtained.

Statistical Atlases

We superimposed all segmented regions of interest to obtain a 3D location and frequency map based on different parameters of interest. Each map computed the frequency occurrence at each voxel in the template space. We then color-coded the frequency for visualization using open-source MRIcroGL software (2018, University of South Carolina–Columbia, SC; *https://www.mccauslandcenter.sc.edu/mricrogl/*).

Group analyses included sex (women, men), age (median as the cut-off), clinical presentation (neurologic deficit, signs of increased intracranial pressure, epileptic seizures), Karnofsky performance status (70% as the cut-off), classification of glioblastoma according to the revised Radiation Therapy Oncology Group–Recursive Partitioning Analysis (RTOG-RPA) classification system (3–6,18), subventricular zone involvement (yes, no), MGMT promoter methylation status (methylated, nonmethylated), extent of surgical resection (biopsy, partial resection, subtotal, and gross total resection), PFS (median as the cut-off), and OS (median as the cut-off). Patient survival rates (PFS, OS) were calculated by using the Kaplan-Meier method.

Statistical Analysis

We analyzed the correlation between segmentations (initial evaluator vs external evaluator) by using the Pearson coefficient. The statistical relationships between region of interest and parameters of interest on a voxel-by-voxel basis were studied with a voxel-based lesion symptom mapping procedure. Each voxel was qualified as inside or outside the region of interest and correlated with a given parameter of interest. We used the Liebermeister statistical test for binary data and the generalized linear model for continuous data. Results of univariable analyses were further corrected by using a multiple comparison permutation test (n = 5000). Voxel t values that were greater than the t value in more than 95% of permutations were retained in the voxel-based lesion symptom mapping results. $P < .05$ was considered indicative of a statistically significant difference. Except for the Pearson coefficient, statistical analysis was performed with open-source software (NiiStat, version 9.0, 2018; University of South Carolina–Columbia, SC; *http://www.nitrc.org/projects/niistat*). The Pearson coefficient was calculated by using commercially available software (JMP, version 14.1.0; SAS Institute, Cary, NC).

Results

Patient Characteristics

The characteristics of the 392 patients (mean age ± standard deviation, 61 years ± 13; 233 men) are detailed in the Table. Of the 392 patients, 233 (59%) were men and 208 (53%) were older than 60 years. The mean Karnofsky performance status at diagnosis was 79.1% ± 13.1, and 197 of the 392 patients (50%) had RTOG-RPA class 3–4 glioblastoma. The most common presenting symptom was neurologic focal deficit (206 of the 392 patients [52%]), followed by epileptic seizure (102 patients [26%]) and signs of increased intracranial pressure (81 patients [21%]). The mean tumor volume was 37.1 cm^3 ± 34.4, and the main location was on the frontal lobe in 138 of the 392 patients (35%) and on the temporal lobe in 124 (32%). A cortical involvement was found in 306 of the 392 patients (78%) and a subventricular zone involvement was found in 248 (63%). A subtotal or gross total resection was performed in 173 of the 392 patients (44%), partial resection was performed in 36 (9%), and biopsy was performed in 183 (47%). MGMT promoter methylation status was assessed in 160 of the 392 patients (41%); 74 glioblastomas (46%) had a methylation of the MGMT promoter.

Quality Assessment

No manual corrections had to be made in the segmentation and the spatial normalization procedures. We observed a strong interevaluator agreement for glioblastoma segmentation by number of voxels (enhancing component: r = 0.96, $P < .001$; necrotic com-

Main Characteristics of the Study Sample

Parameter	Value
Clinical characteristics at diagnosis	
Sex	
Women	159 (41)
Men	233 (59)
Age (y)	
Mean ± standard deviation	61 ± 13
≤60	`184 (47)
>60	208 (53)
Karnofsky performance status at diagnosis (%)	
Mean ± standard deviation	79.1 ± 13.1
≥70	348 (89)
<70	44 (11)
RTOG-RPA class	
3–4	197 (50)
5–6	195 (49)
Presenting symptom	
Incidental	3 (1)
Epileptic seizure	102 (26)
Signs of increased intracranial pressure	81 (21)
Neurologic focal deficit	206 (52)
MRI characteristics at diagnosis	
Main lobar location	
Frontal	138 (35)
Temporal	124 (32)
Parietal	90 (23)
Insular	8 (2.0)
Other	32 (8)
Cortex involvement	
No	86 (22)
Yes	306 (78)
Subventricular zone involvement	
No	144 (37)
Yes	248 (63)
Tumor volume of the contrast enhancement (cm^3)	
Mean ± standard deviation	37.1 ± 34.4
<40	248 (63)
≥40	144 (37)
Molecular characteristics	
MGMT promoter status	
No	86 (22)
Yes	74 (19)
Not available	232 (59)
Treatment-related characteristics	
Surgical treatment	
Biopsy	183 (47)
Partial resection	36 (9)
Subtotal and gross total resection	173 (44)

Table 1 *(continues)*

Table *(continued)*: Main Characteristics of the Study Sample

Parameter	Value
Survival characteristics	
Progression-free survival (mo)*	
Median	7.5 (7.0, 13.5)
<7.5	174 (44)
≥7.5	177 (45)
Overall survival (mo)†	
Median	14.4 (12.2, 24.9)
<14.4	171 (44)
≥14.4	163 (42)

Note.—Except where indicated, data are numbers of patients (n = 392), with percentages in parentheses. MGMT = O^6-methylguanine DNA methyltransferase methylation, RTOG-RPA = revised Radiation Therapy Oncology Group–Recursive Partitioning Analysis.

* Forty-one patients with an available follow-up of less than 7.5 months and without observed tumor progression were not included in this analysis. Numbers in parentheses are the 95% confidence interval.

† Fifty-eight patients with an available follow-up of less than 14.4 months and without observed death from oncologic cause were not included in this analysis. Numbers in parentheses are the 95% confidence interval.

ponent: $r = 0.92$, $P < .001$; whole lesion component: $r = 0.96$, $P < .001$). The mean distance of the parenchymal landmarks between the Montreal Neurologic Institute template and the normalized sequences was 3.8 mm ± 7.3 (range, 0.5–9.9 mm; median, 2.5 mm; interquartile range, 2.0 mm) (Table E1 [online]). Regarding the clinical validation, location and frequency maps and statistical probabilistic maps of IDH wild-type glioblastomas according to sex (Figs E3–E5 [online]) and Karnofsky performance status at diagnosis (Figs E6–E8 [online]) were in line with those previously published (11,17,19).

Glioblastoma Location

We found the highest prevalence of IDH wild-type glioblastomas in the subcortical white matter of the subventricular zones of both hemispheres (248 of 392 patients, 63%) (Fig 2).

We found differences in glioblastoma location according to the subventricular zone involvement ($P < .05$) (Fig E11 [online]). In the 248 patients with subventricular zone involvement, glioblastomas had a higher probability of being located in the anterior horn (33 patients, 13%); right (56 patients, 23%) and left (41 patients, 16%) atrium; and right (38 patients, 15%) and left (26 patients, 10%) temporal horn of lateral ventricles ($P < .05$) (Figs E9, E11 [online]). In the 144 patients with no subventricular zone involvement (37%), glioblastomas had a higher probability of being located in the right (16 patients, 11%) and left (15 patients, 10%) inferior frontal gyri; right (13 patients, 9%) and left (10 patients, 7%) pre- and postcentral gyri; right (13 patients, 9%) and left (10 patients, 7%) superior parietal lobules; and right superior temporal gyrus (14 patients, 10%) ($P < .05$) (Figs E10, E11 [online]).

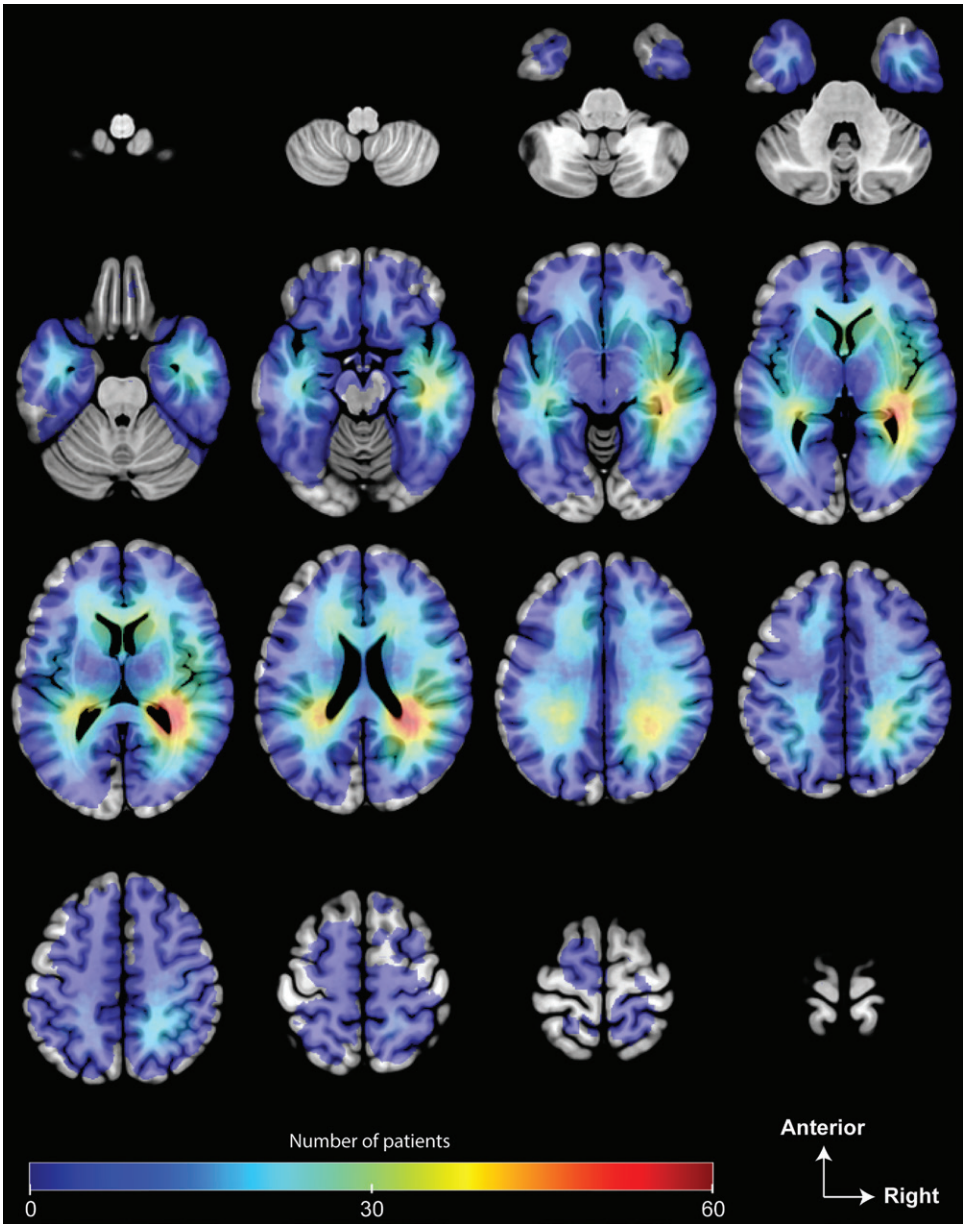

Figure 2: Location and frequency of isocitrate dehydrogenase (IDH) wild-type glioblastoma (*n* = 392). Color frequency map illustrates location of and number of patients with IDH wild-type glioblastoma. Images are displayed in neurologic display convention.

Age

We found differences in glioblastoma location according to the age at diagnosis ($P < .05$) (Fig E14 [online]). In the 208 patients older than 60 years (53%), glioblastomas had a higher probability of being located in the left inferior frontal gyrus (11 patients, 5%), left insular lobe (14 patients, 7%), left temporal pole (11 patients, 5%), right medial orbital gyrus (10 patients, 5%), right internal capsule (18 patients, 9%), right globus pallidus (16 patients, 8%), and right inferior parietal lobule (20 patients, 10%) ($P < .05$) (Figs E12, E14 [online]). In the 184 patients younger than 60 years (47%), glioblastomas had a higher probability of being located in the diencephalo-mesencephalon (nine patients, 5%); left middle (11 patients, 6%) and superior (15 patients, 8.2%) temporal gyri; right inferior temporal gyrus (13 patients, 7.1%); right fusiform and parahippocampal gyri (20 patients, 11%); right inferior (12 patients, 6%), middle (12 patients, 6%), and superior (10 patients, 5%) frontal gyri; right insular lobe (20 patients, 11%); left superior frontal gyrus (eight patients, 4%); right inferior parietal lobule (14 patients, 8%); and left postcentral gyrus (14 patients, 8%) ($P < .05$) (Figs E13, E14 [online]).

Clinical Presentation

We found differences in glioblastoma location according to the clinical presentation ($P < .05$) (Fig 3). In the 102 patients for whom the glioblastoma was revealed because of epileptic seizures (26%), glioblastomas had a greater probability of location in the right superior (13 patients, 13%), middle (10 patients, 10%), and inferior (nine patients, 9%) temporal gyri; right fusiform and parahippocampal gyri (13 patients, 13%); right pre- and postcentral gyri (10 patients, 10%); right (seven patients, 7%) and left (five patients, 5%) cingulate gyri; left superior frontal gyrus (four patients, 4%); left postcentral gyrus (five patients, 5%); and right middle frontal gyrus (five patients, 5%) ($P < .05$) (Figs 3, E15 [online]). In the 206 patients for whom the glioblastoma was revealed because of a focal neurologic deficit (52%), glioblastomas had a higher probability of being located in the right (26 patients, 13%) and left (22 patients, 11%) pre- and postcentral gyri; right (50 patients, 24%) and left (42 patients, 20%) fronto-parieto-temporal areas; left superior temporal gyrus (21 patients, 10%); left fusiform and parahippocampal gyri (24 patients, 12%); left insular lobe (21 patients, 10%); posterior part of the right (31 patients, 15%) and left (27 patients, 13%) internal capsules; and right (41 patients, 20%) and left (36 patients, 18%) deep gray nuclei ($P < .05$) (Figs 3, E16 [online]).

In the 81 patients for whom the glioblastoma was revealed by signs of increased intracranial pressure (21%), glioblastomas had a higher probability of being located in the right frontal lobes (21 patients, 26%), temporal lobes (23 patients, 28%),

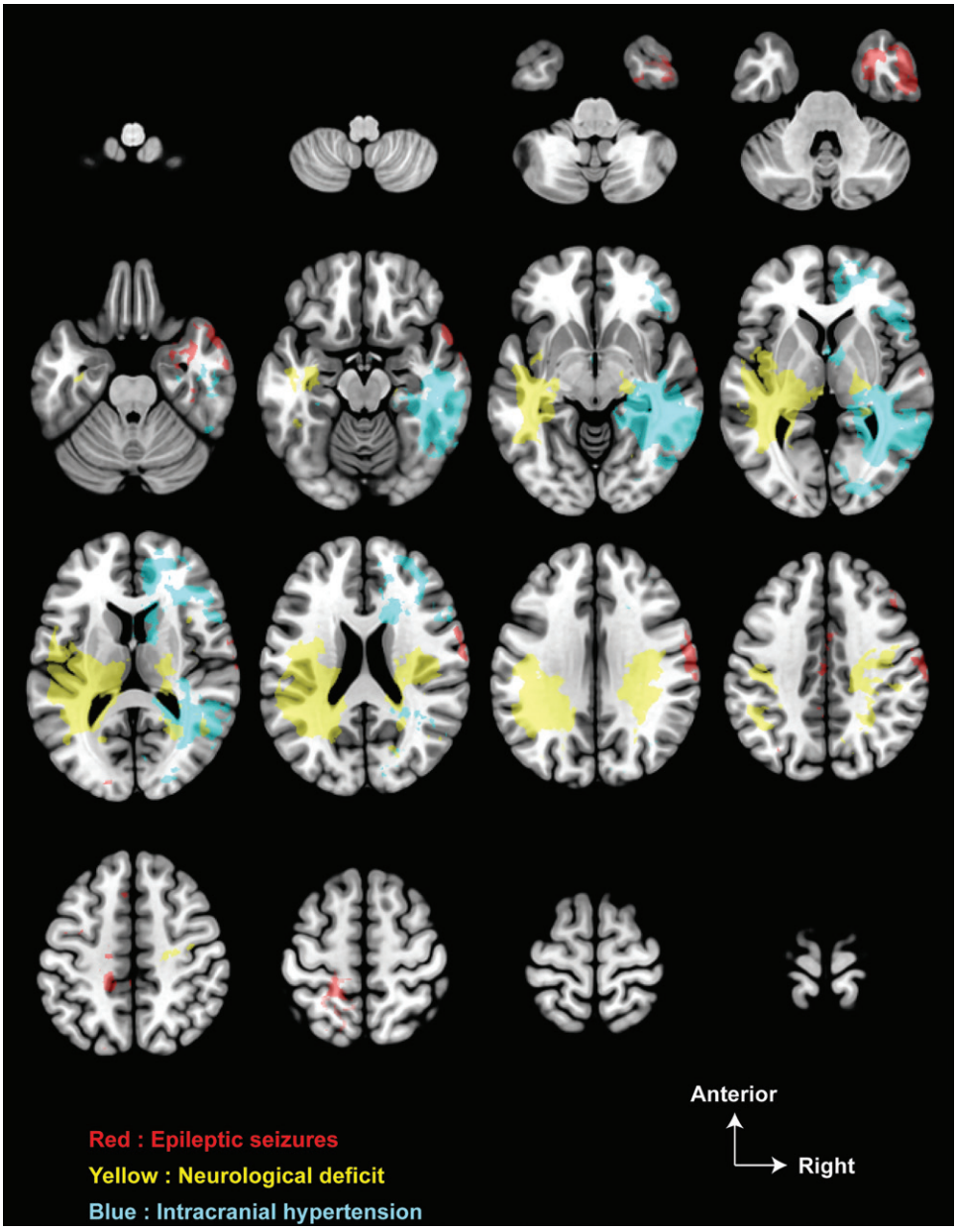

Figure 3: Probability map of isocitrate dehydrogenase (IDH) wild-type glioblastoma location according to clinical presentation. IDH wild-type glioblastomas show a difference in location ($P < .05$) between patients with epileptic seizures at clinical presentation (102 of 392 patients [26%], in red), patients with a neurologic focal deficit at clinical presentation (206 of 392 patients [52%], in yellow), and patients with signs of increased intracranial pressure at clinical presentation (81 of 392 patients [21%], in blue). The three patients (0.8%) with an incidental discovery of their IDH wild-type glioblastomas were not included. Images are displayed in neurologic display convention.

occipital lobes (17 patients, 21%), right caudate nucleus (22 patients, 27%), anterior part of the right internal capsule (12 patients, 15%), corpus callosum (20 patients, 25%), and right temporo-occipital area (34 patients, 42%) ($P < .05$) (Figs 3, E17 [online]).

RTOG-RPA Classification System

We found differences in glioblastoma location according to the RTOG-RPA classes ($P < .05$) (Fig E20 [online]). In the 195 patients with RTOG-RPA classes 5–6 (50%), glioblastomas had a higher probability of being located in the corpus callosum (23 patients, 12%); right (23 patients, 12%) and left (16 patients, 8%) deep gray nuclei; right (11 patients, 6%) and left (10 patients, 5%) orbital gyri; left pre- and postcentral gyri (16 patients, 8%); left superior (13 patients, 7%) and middle (16 patients, 8%) frontal gyri; right (19 patients, 10%) and left (22 patients, 11%) cingulate gyri; fusiform and parahippocampal gyri (14 patients, 7%); left insular lobe (11 patients, 6%); left external capsule (11 patients, 6%); and right superior frontal gyrus (six patients, 3%) ($P < .05$) (Figs E18, E20 [online]).

In the 197 patients with RTOG-RPA classes 3–4 (50%), glioblastomas had a higher probability of being located in the right inferior (13 patients, 7%) and middle (14 patients, 7%) frontal gyri; left middle temporal gyrus (11 patients, 6%); right superior (23 patients, 12%) and middle (19 patients, 10%) temporal gyri; right precentral gyrus (15 patients, 8%); right (20 patients, 10%) and left (14 patients, 7%) postcentral gyri; right (15 patients, 8%) and left (11 patients, 6%) superior parietal lobules; and right inferior parietal lobule (22 patients, 11%) ($P < .05$) (Figs E19, E20 [online]).

MGMT Promoter Methylation Status

We found no differences in glioblastoma location according to MGMT promoter methylation status ($P > .05$) (Figs E21, E22 [online]).

Surgical Management

We found differences in glioblastoma location according to the surgical management ($P < .05$) (Fig E23 [online]). In the 183 patients for whom a biopsy was performed (47%), glioblastomas had a higher probability of being located in the right (19 patients, 10%) and left (29 patients, 16%) deep gray nuclei; corpus callosum (21 patients, 12%); left internal capsule (13 patients, 7%); left pre- and postcentral gyri (15 patients, 8%); left insular lobe (12 patients, 7%); left superior frontal gyrus (11 patients, 6%); left orbital gyri (nine patients, 5%); right (18 patients, 10%) and

left (22 patients, 12%) cingulate gyri; and right precentral gyrus (11 patients, 6%) ($P < .05$) (Figs E23, E24 [online]).

In the 36 patients for whom a partial surgical resection was performed (9%), glioblastomas had a higher probability of being located in the left middle (five patients, 14%) and superior (five patients, 14%) frontal gyri; right (five patients, 14%) and left (four patients, 11%) precentral gyri; right internal capsule (seven patients, 19%); right (seven patients, 19%) and left (five patients, 14%) lenticular nucleus; right external capsule (seven patients, 19%); right (seven patients, 19%) and left (five patients, 14%) insular lobes; left orbital gyri (three patients, 8%); right (four patients, 11%) and left (five patients, 14%) cingulate gyri; left superior (five patients, 14%) and middle (five patients, 14%) temporal gyri; right temporal pole (six patients, 17%); right hippocampal gyrus (six patients, 17%); right cuneus (three patients, 8%); and right superior parietal lobule (four patients, 11%) ($P < .05$) (Figs E23, E25 [online]).

In the 173 patients for whom a subtotal or a gross total surgical resection was performed (44%), glioblastomas had a higher probability of being located in the right temporal lobe (26 patients, 15%); right (17 patients, 10%) and left (10 patients, 6%) superior parietal lobules; right (20 patients, 12%) and left (12 patients, 7%) inferior parietal lobules; right frontal lobe (14 patients, 8%); left occipital lobe (10 patients, 6%); left lingual gyrus (10 patients, 6%); left inferior frontal gyrus (six patients, 4%); and right (15 patients, 9%) and left (seven patients, 4%) inferior temporal gyri ($P < .05$) (Figs E23, E26 [online]).

Survival Analysis

During the follow-up (mean, 14.5 months ± 13.1), 332 of the 392 patients (85%) had tumor progression (60 censored patients) and 292 (74%) died (100 censored patients). The median PFS was 7.5 months (95% confidence interval [CI]: 7.0 months, 13.5 months), and the median OS was 14.4 months (95% CI: 12.2 months, 16.5 months). Survival curves are presented in Figure 4. We observed similar results between statistical probabilistic maps of glioblastoma location by PFS and by OS as continuous data and as binary data.

We found differences in glioblastoma location according to the PFS ($P < .05$) (Fig 5). Subgroup analyses stratified according to location (frontal, temporal) and extent of surgical resection (biopsy, surgical resection) are detailed in Figures E27–E30 (online). In the 174 patients with a short PFS (50%), glioblastomas had a higher probability of being located in the right (21 patients, 12%) and left (13 patients, 8%) lenticular nuclei; right thalamic nucleus (22 patients, 13%); corpus callosum (22 patients, 13%); right insular lobe (17 patients, 10%); right superior temporal gyrus (19 patients, 11%); and right (15 patients, 9%) and left (17 patients, 10%) frontal lobes ($P < .05$) (Figs 5, E31 [online]).

In the 177 patients with a long PFS (50%), glioblastomas had a higher probability of being located in the right superior (six patients, 3%) and middle (10 patients, 6%) frontal gyri; left middle temporal gyrus (nine patients, 5%); right precentral gyrus (13 patients, 7%); right inferior parietal lobule (17 patients, 10%); right superior temporal gyrus (21 patients, 12%); right middle temporal gyrus (22 patients, 12%); and right occipital lobe (14 patients, 8%) ($P < .05$) (Figs 5, E32 [online]).

We found differences in glioblastoma location according to the OS ($P < .05$) (Fig 6). Subgroup analyses stratified according to location (frontal, temporal) and extent of surgical resection (biopsy, surgical resection) are detailed in Figures E33–E36 (online). In the 171 patients with a short OS (44%), glioblastomas had a higher probability of being located in the right (22 patients, 13%) and left (13 patients, 8%) lenticular nuclei; right thalamic nucleus (24 patients, 14%); corpus callosum (21 patients, 12%); right insular lobe (18 patients, 9%); right superior temporal gyrus (17 patients, 10%); left superior frontal gyrus (10 patients, 6%); right middle frontal gyrus (10 patients, 6%); left postcentral gyrus (17 patients, 10%); and left fusiform gyrus (11 patients, 6%) ($P < .05$) (Figs 6, E37 [online]).

In the 163 patients with a long OS (42%), glioblastomas had a higher probability of being located in the right superior (seven patients, 4%) and middle (10 patients, 6%) frontal gyri; right (seven patients, 4%) and left (six patients, 4%) inferior frontal gyri; right pre- and postcentral gyri (14 patients, 9%); right inferior parietal lobule (18 patients, 11%); left inferior temporal gyrus (10 patients, 6%); and right occipital lobe (12 patients, 7%) ($P < .05$) (Figs 6, E38 [online]).

Discussion

We developed a three-dimensional (3D) atlas of glioblastoma location based on a homogeneous clinical, MRI, and histopathologic database of 392 newly diagnosed isocitrate dehydrogenase (IDH) wild-type supratentorial glioblastomas in adults. We built a convenient semiautomated process that can be reproduced, allowing probabilistic analyses to be performed by using only a 3D T1-weighted fast spoiled gradient-recalled MRI sequence. This statistical probabilistic map approach illustrates that glioblastoma location recapitulates main prognostic factors, helps determine subsequent neurosurgical management, and correlates with patient survival. We showed that a superficial location distant from the eloquent area was associated with a preserved functional status at diagnosis (348 of 392 patients [89%], $P < .05$), a subtotal or gross total surgical resection (173 of 392 patients [44%], $P < .05$), and prolonged survival (177 of 332 patients [53%] for progression-free survival [PFS] and 163 of 334 patients [42%] for overall survival [OS]; $P < .05$). In comparison, deep tumor location and a location within eloquent brain areas were associated with an impaired functional status at diagnosis (44 of 392 patients [11%], $P < .05$), neurologic deficit (206 of 392 patients [52%], $P < .05$), surgical management with biopsy only (183 of 392 patients [47%], $P < .05$), and shortened survival (174 of 351 patients [44%] for PFS and 171 of 334 patients [44%] for OS; $P < .05$).

In contrast to previous reports (10,20), which found a high prevalence of glioblastomas in the posterior part of the subventricular zone, we identified three preferential clusters for glioblastoma location involving the lateral ventricles: anterior horn, atrium, and temporal horn, in line with the subventricular zone concept (21,22). Regarding the statistical probabilistic map of glioblastoma location according to Karnofsky performance

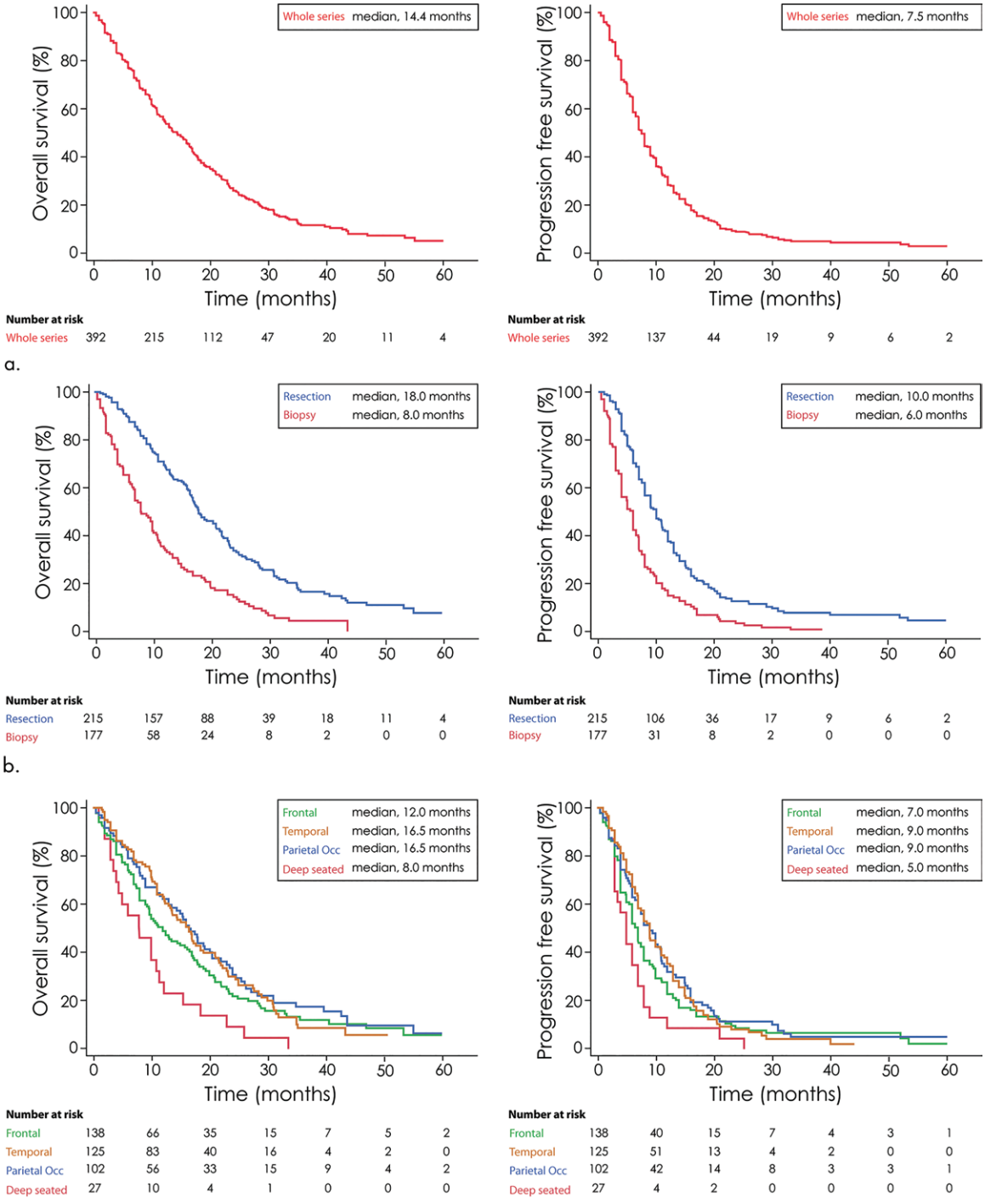

Figure 4: Kaplan-Meier estimates of overall survival (OS) and progression-free survival (PFS). **(a)** OS (left) and PFS (right) in the whole series (n = 392). **(b)** OS (left) and PFS (right) according to surgical treatment (resection vs biopsy). The unadjusted hazard ratio for PFS with resection compared to biopsy was 0.51 (95% confidence interval [CI]: 0.41, 0.64; $P < .001$). The unadjusted hazard ratio for OS with resection compared to biopsy was 0.45 (95% CI: 0.35, 0.57; $P < .001$). **(c)** OS and PFS according to glioblastoma location (frontal vs temporal vs parietal and occipital [occ] vs deep-seated). The unadjusted hazard ratio for PFS in the frontal subgroup, as compared with the deep-seated subgroup, was 0.63 (95% CI: 0.41, 0.99; $P = .048$). The unadjusted hazard ratio for PFS in the temporal subgroup, as compared with the deep-seated subgroup, was 0.55 (95% CI: 0.34, 0.86; $P = .009$). The unadjusted hazard ratio for PFS in the parietal and occipital subgroup, as compared with the deep-seated subgroup, was 0.52 (95% CI: 0.33, 0.83; $P = .006$). The unadjusted hazard ratio for OS in the frontal subgroup, as compared with the deep-seated subgroup, was 0.56 (95% CI: 0.35, 0.87; $P = .011$). The unadjusted hazard ratio for OS in the temporal subgroup, as compared with the deep-seated subgroup, was 0.46 (95% CI: 0.29, 0.74; $P = .001$). The unadjusted hazard ratio for OS in the parietal and occipital subgroup, as compared with the deep-seated subgroup, was 0.43 (95% CI: 0.27, 0.70; $P < .001$).

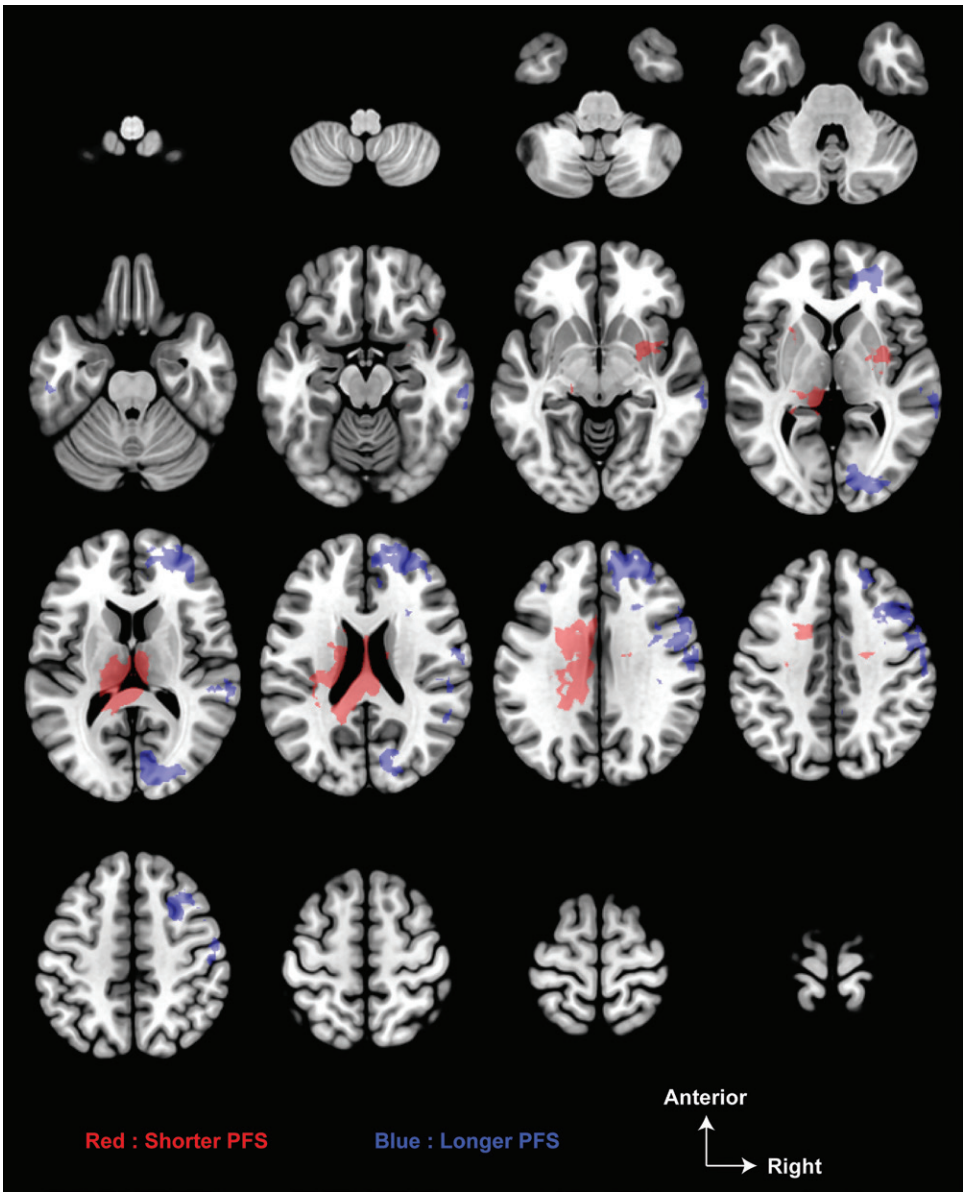

Figure 5: Probability map of isocitrate dehydrogenase (IDH) wild-type glioblastoma location according to progression-free survival (PFS). The probability map of IDH wild-type glioblastoma location according to PFS shows a difference in location ($P < .05$) between patients with a PFS shorter than 7.5 months (174 of 351 patients [44%], in red) and patients with a PFS longer than 7.5 months (177 of 351 patients [47%], in blue). Images are displayed in neurologic display convention.

status, we found that impaired Karnofsky performance status at diagnosis was associated with midline areas and involvement of left precentral areas. Similarly, Marina et al (23) found a thalamic location or corpus callosum involvement in 27% of patients with glioblastoma and impaired Karnofsky performance status at diagnosis, whereas Chaichana et al (24) found a midline location in only 11% of patients with a Karnofsky performance status at diagnosis of 70% or higher. We found that IDH wild-type glioblastomas more likely involved both hemispheres in patients aged 60 years and older, and we found a more likely midline involvement in younger patients and in women. These results suggest a particular histomolecular subtype for IDH wild-type glioblastomas involving the midline in younger patients, as for diffuse midline H3 K27M-mutant pediatric high-grade gliomas (26,26) and in women (27).

Contrary to previous reports (9,28,29), we found no preferential IDH wild-type glioblastoma location according to MGMT promoter status. This may be related to the small sample of patients with an available MGMT status or to the exclusion of IDH-mutant glioblastomas in our study but not in previous studies. Even if a difference in spatial distribution according to MGMT promoter methylation status were to be confirmed in a larger size cohort, the spatial overlap would limit its diagnostic or prognostic value. This requires further validation. We observed that the surgical procedure and the extent of resection were influenced by the glioblastoma location, in accordance with the literature, where surgical decision making was reported to depend on tumor location (5), functional status, age, and patient expectations (30). We observed that both PFS and OS were impacted by tumor location. Interestingly, the survival probability maps overlapped those of other prognostic parameters, including functional status at diagnosis, and extent of surgical resection, providing an integration of multimodal information impacting survival results, which could be helpful for daily practice.

Our study has some limitations. The retrospective and monocentric design, without an external validation set, limits the generalizability of the proposed atlas. Patients with a putative glioblastoma without histopathologic confirmation, who constituted a subset of patients with a poorer prognosis, were excluded. In addition, the lack of tissue samples for further biomolecular analyses did not allow the determination of epidermal growth factor receptor variant III status and gene-based molecular classification (10,11,31) and explains why the MGMT promoter status was available in only approximately 41% of patients. We introduced a cost function masking approach in our spatial normalization procedure to reduce the tumor-induced mass effect (15). The presence of a clinically relevant glioblastoma-induced mass effect may have limited the spatial normalization procedure. To control for this bias, we used validated tumor nonlinear transformations methods to register MRI data into the Montreal

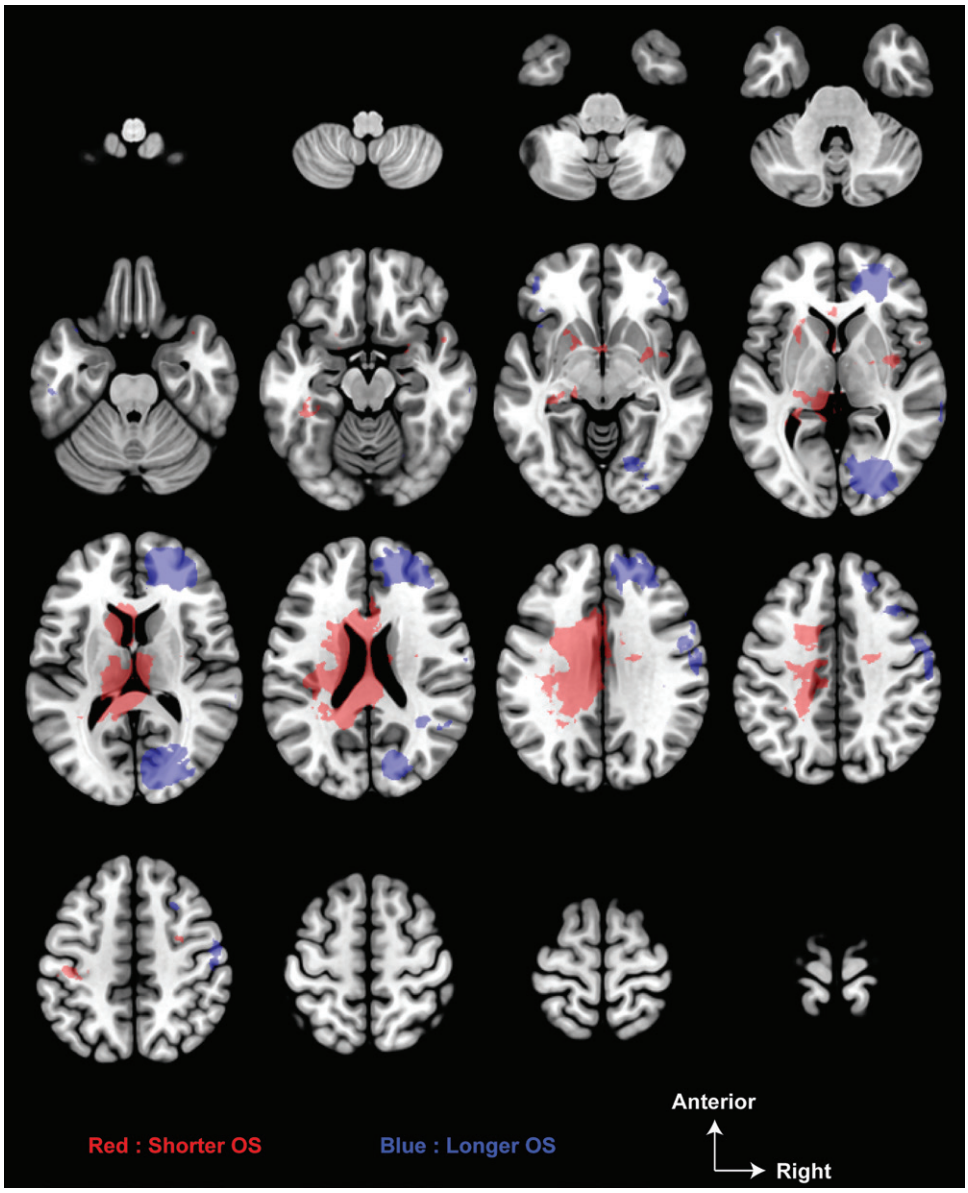

Figure 6: Probability map of isocitrate dehydrogenase (IDH) wild-type glioblastoma location according to overall survival (OS). IDH wild-type glioblastomas show a difference in location ($P < .05$) between patients with an OS shorter than 14.4 months (171 of 334 patients [51%], in red) and patients with an OS longer than 14.4 months (163 of 334 patients [49%], in blue). Images are displayed in neurologic display convention.

Neurologic Institute template, offering a higher localization accuracy (14). No other available spatial normalization procedure accounts for tumor-induced mass effect based only on a clinical MRI sequence (14,15,32), enantiomorphic transformation being unsuitable for potential bilateral or multifocal lesions, such as glioblastomas (33) and the Glioma Image Segmentation and Registration software requiring four MRI sequences (11).

In conclusion, this three-dimensional (3D) MRI-based atlas through probabilistic analysis identified the preferential isocitrate dehydrogenase wild-type glioblastoma location according to parameters of interest and provided an image-based integration of multimodal information impacting survival results. Because the known prognostic parameters appear to be related to the glioblastoma location, the 3D location parameter should be incorporated into prognostic scoring systems. In addition, it should refine clinical management and treatment planning. For example, it may help tailor antiepileptic drug prophylaxis in patients at high risk of epileptic seizures. Future developments will help radiomic analyses to identify new theranostic markers and help decision making by estimating preoperatively both resectability and the risks of postoperative neurologic deficits in a given patient.

Acknowledgments: Alexandre Roux thanks the French Society of Neurosurgery and the Nuovo-Soldati Foundation for Cancer Research for their support. Johan Pallud thanks the Cancéropôle Ile-de-France for their support.

Author contributions: Guarantors of integrity of entire study, A.R., E.D., F.C., J.P.; study concepts/study design or data acquisition or data analysis/interpretation, all authors; manuscript drafting or manuscript revision for important intellectual content, all authors; approval of final version of submitted manuscript, all authors; agrees to ensure any questions related to the work are appropriately resolved, all authors; literature research, A.R., M.E., M.Z., E.D., P.G., S.L., A.F., J.F.M., F.C., P.V., C.O., J.P.; clinical studies, A.R., E.D., S.L., F.D., F.C., E.L., P.V., C.O., J.P.; experimental studies, E.D., P.G., E.L., P.V., J.P.; statistical analysis, A.R., P.R., K.S., E.D., P.G., A.F., P.V., J.P.; and manuscript editing, A.R., P.R., M.E., K.S., M.Z., E.D., P.G., F.D., F.C., E.L., P.V., C.O., J.P.

Disclosures of Conflicts of Interest: **A.R.** disclosed no relevant relationships. **P.R.** disclosed no relevant relationships. **M.E.** disclosed no relevant relationships. **K.S.** disclosed no relevant relationships. **M.Z.** disclosed no relevant relationships. **E.D.** disclosed no relevant relationships. **P.G.** disclosed no relevant relationships. **S.L.** disclosed no relevant relationships. **A.F.** disclosed no relevant relationships. **F.D.** disclosed no relevant relationships. **J.F.M.** disclosed no relevant relationships. **F.C.** disclosed no relevant relationships. **E.L.** disclosed no relevant relationships. **P.V.** Activities related to the present article: disclosed no relevant relationships. Activities not related to the present article: institution receives money for board membership at Novartis, Boeringer-Ingelheim, and Hoffman-LaRoche; institution has grants/grants pending at LaLigue Contre le Cancer, and SFCE; receives payment for lectures including service on speakers bureaus from IPSEN. Other relationships: disclosed no relevant relationships. **C.O.** disclosed no relevant relationships. **J.P.** disclosed no relevant relationships.

References

1. Louis DN, Ohgaki H, Wiestler OD, et al. WHO Classification of Tumours of the Central Nervous System. Revised 4th ed. Geneva, Switzerland: World Health Organization, YEAR.
2. Simpson JR, Horton J, Scott C, et al. Influence of location and extent of surgical resection on survival of patients with glioblastoma multiforme: results of three consecutive Radiation Therapy Oncology Group (RTOG) clinical trials. Int J Radiat Oncol Biol Phys 1993;26(2):239–244.

3. Pallud J, Roux A, Zanello M. Relationship between tumour location and preoperative seizure incidence depends on glioma grade of malignancy. Epileptic Disord 2016;18(1):107–108.
4. Awad AW, Karsy M, Sanai N, et al. Impact of removed tumor volume and location on patient outcome in glioblastoma. J Neurooncol 2017;135(1):161–171.
5. Woo P, Ho J, Lam S, et al. A Comparative Analysis of the Usefulness of Survival Prediction Models for Patients with Glioblastoma in the Temozolomide Era: The Importance of Methylguanine Methyltransferase Promoter Methylation, Extent of Resection, and Subventricular Zone Location. World Neurosurg 2018;115:e375–e385.
6. Paldor I, Pearce FC, Drummond KJ, Kaye AH. Frontal glioblastoma multiforme may be biologically distinct from non-frontal and multilobar tumors. J Clin Neurosci 2016;34:128–132.
7. De Witt Hamer PC, Hendriks EJ, Mandonnet E, Barkhof F, Zwinderman AH, Duffau H. Resection probability maps for quality assessment of glioma surgery without brain location bias. PLoS One 2013;8(9):e73353.
8. Parisot S, Darlix A, Baumann C, et al. A Probabilistic Atlas of Diffuse WHO Grade II Glioma Locations in the Brain. PLoS One 2016;11(1):e0144200.
9. Ellingson BM, Cloughesy TF, Pope WB, et al. Anatomic localization of O6-methylguanine DNA methyltransferase (MGMT) promoter methylated and unmethylated tumors: a radiographic study in 358 de novo human glioblastomas. Neuroimage 2012;59(2):908–916.
10. Ellingson BM, Lai A, Harris RJ, et al. Probabilistic radiographic atlas of glioblastoma phenotypes. AJNR Am J Neuroradiol 2013;34(3):533–540.
11. Bilello M, Akbari H, Da X, et al. Population-based MRI atlases of spatial distribution are specific to patient and tumor characteristics in glioblastoma. Neuroimage Clin 2016;12:34–40.
12. Kickingereder P, Bonekamp D, Nowosielski M, et al. Radiogenomics of Glioblastoma: Machine Learning-based Classification of Molecular Characteristics by Using Multiparametric and Multiregional MR Imaging Features. Radiology 2016;281(3):907–918.
13. Stupp R, Mason WP, van den Bent MJ, et al. Radiotherapy plus concomitant and adjuvant temozolomide for glioblastoma. N Engl J Med 2005;352(10):987–996.
14. Ripollés P, Marco-Pallarés J, de Diego-Balaguer R, et al. Analysis of automated methods for spatial normalization of lesioned brains. Neuroimage 2012;60(2):1296–1306.
15. Brett M, Leff AP, Rorden C, Ashburner J. Spatial normalization of brain images with focal lesions using cost function masking. Neuroimage 2001;14(2):486–500.
16. Lee JW, Wen PY, Hurwitz S, et al. Morphological characteristics of brain tumors causing seizures. Arch Neurol 2010;67(3):336–342.
17. Li HY, Sun CR, He M, Yin LC, Du HG, Zhang JM. Correlation Between Tumor Location and Clinical Properties of Glioblastomas in Frontal and Temporal Lobes. World Neurosurg 2018;112:e407–e414 [Published correction appears in World Neurosurg 2018;115:512.] https://doi.org/10.1016/j.wneu.2018.01.055.
18. Mirimanoff RO, Gorlia T, Mason W, et al. Radiotherapy and temozolomide for newly diagnosed glioblastoma: recursive partitioning analysis of the EORTC 26981/22981-NCIC CE3 phase III randomized trial. J Clin Oncol 2006;24(16):2563–2569.
19. Chang EF, Smith JS, Chang SM, et al. Preoperative prognostic classification system for hemispheric low-grade gliomas in adults. J Neurosurg 2008;109(5):817–824.
20. Wang Y, Liu S, Fan X, et al. Age-associated brain regions in gliomas: a volumetric analysis. J Neurooncol 2015;123(2):299–306.
21. Sanai N, Tramontin AD, Quiñones-Hinojosa A, et al. Unique astrocyte ribbon in adult human brain contains neural stem cells but lacks chain migration. Nature 2004;427(6976):740–744.
22. Sanai N, Alvarez-Buylla A, Berger MS. Neural stem cells and the origin of gliomas. N Engl J Med 2005;353(8):811–822.
23. Marina O, Suh JH, Reddy CA, et al. Treatment outcomes for patients with glioblastoma multiforme and a low Karnofsky Performance Scale score on presentation to a tertiary care institution: Clinical article. J Neurosurg 2011;115(2):220–229.
24. Chaichana KL, Jusue-Torres I, Navarro-Ramirez R, et al. Establishing percent resection and residual volume thresholds affecting survival and recurrence for patients with newly diagnosed intracranial glioblastoma. Neuro Oncol 2014;16(1):113–122.
25. Schwartzentruber J, Korshunov A, Liu XY, et al. Driver mutations in histone H3.3 and chromatin remodelling genes in paediatric glioblastoma. Nature 2012;482(7384):226–231 [Published correction appears in Nature 2012;484(7392):130.] https://doi.org/10.1038/nature10833.
26. Wu G, Diaz AK, Paugh BS, et al. The genomic landscape of diffuse intrinsic pontine glioma and pediatric non-brainstem high-grade glioma. Nat Genet 2014;46(5):444–450.
27. Yang W, Warrington NM, Taylor SJ, et al. Sex differences in GBM revealed by analysis of patient imaging, transcriptome, and survival data. Sci Transl Med 2019;11(473):eaao5253.
28. Han Y, Yan LF, Wang XB, et al. Structural and advanced imaging in predicting MGMT promoter methylation of primary glioblastoma: a region of interest based analysis. BMC Cancer 2018;18(1):215.
29. Eoli M, Menghi F, Bruzzone MG, et al. Methylation of O6-methylguanine DNA methyltransferase and loss of heterozygosity on 19q and/or 17p are overlapping features of secondary glioblastomas with prolonged survival. Clin Cancer Res 2007;13(9):2606–2613.
30. Sonabend AM, Zacharia BE, Cloney MB, et al. Defining Glioblastoma Resectability Through the Wisdom of the Crowd: A Proof-of-Principle Study. Neurosurgery 2017;80(4):590–601.
31. Verhaak RGW, Hoadley KA, Purdom E, et al. Integrated genomic analysis identifies clinically relevant subtypes of glioblastoma characterized by abnormalities in PDGFRA, IDH1, EGFR, and NF1. Cancer Cell 2010;17(1):98–110.
32. Crinion J, Ashburner J, Leff A, Brett M, Price C, Friston K. Spatial normalization of lesioned brains: performance evaluation and impact on fMRI analyses. Neuroimage 2007;37(3):866–875.
33. Nachev P, Coulthard E, Jäger HR, Kennard C, Husain M. Enantiomorphic normalization of focally lesioned brains. Neuroimage 2008;39(3):1215–1226.